Chalcogenide Letters Vol. 21, No. 6, June 2024, p. 475 - 482

Photocatalytic properties of Cu_2CdSnS_4-CdS nanocomposites synthesized via solvothermal method

G. Hao*, S. Xuye, G. Tao, C. Lin
School of Materials Science and Engineering, Yancheng Institute of Technology, Yancheng 224051, PR China

Cu_2CdSnS_4-CdS nanocomposites are successfully prepared via a two-step solvothermal approach. Powder X-ray diffraction (XRD), Scanning electron microscope (SEM), Photoluminescence (PL) spectroscopy and UV-Vis diffuse reflectance spectroscopy are used to characterized the Cu_2CdSnS_4-CdS nanocomposites. The results show that Cu_2CdSnS_4-CdS nanocomposites present nanoflower structure self-assembling by nanosheets with a thickness of ~50nm and spheroid structure with the average size of 100nm. The band gap is calculated to be 1.5eV. The photodegradation efficiency under visible-light irradiation is reached to 94%, the work provide a new strategy to prepare Cu_2CdSnS_4-CdS nanocomposites for high effective visible-light photocatalytic material.

(Received March 30, 2024, Accepted June 17, 2024)

Keywords: Semiconductors, Cu_2CdSnS_4, CdS, Nanocomposites, Solvothermal, Photocatalytic

1. Introduction

Since the industrial revolution, water contamination has caused a serious and irreparable damage worldwide. A various prospective methods to purify waste water have driven a remarkable interest. Many photocatalysts have been studied to degrade organic pollutants by lowering their band gap to expand the widely photo-response range under natural light conditions. Furthermore, in order to solve the existing problem of rapid recombination of the photogenerated electrons and holes in single semiconductor, the p-type semiconductor is coupled with an n-type semiconductor to construct composite photocatalysts with high enhanced photocatalytic activities by researchers. Among numerous p-type sulfide photocatalysts, Cu_2ZnSnS_4(CZTS) has been drawn considerable attention by the researchers owing to its relatively narrow band gap of about 1.5eV and excellent absorption coefficient of $>10^4 cm^{-1}$ under light irradiation[1]. Transition metal-based Cu_2CdSnS_4(CCTS) quaternary sulfide semiconductor with an optimal band gap of 1.37eV and a high absorption coefficient over 10^4 cm^{-1} is also considered as a possible photocatalytic material owing to its analogous structural and optical properties with CZTS[2]. Cu_2CdSnS_4 materials have been synthesized by some approaches such as microwave irradiation, chemical spray pyrolysis technique, solvothermal synthesis, successive ionic layer adsorption and reaction, thermal decomposition process, direct liquid coating and so on[3-10]. CdS is also one of the most hope-for material in optoelectronic, photovoltaic and photosensitive devices since it possesses a direct band gap of 2.42eV for wurtzite structure and 3.53eV for zinc blende structure. The different shapes and sizes of CdS nanomaterials are synthesized via a variety of techniques including micro-emulsions, sputtering technique, chemical path deposition, stepwise method, solvothermal route, sol-gel

* Corresponding author: guanhao1980@sina.com
https://doi.org/10.15251/CL.2024.216.475

technique, precipitation method and so on[11-17]. The Cu_2CdSnS_4/CdS heterostructure are usually produced by co-sputtering technique, which is mainly studied in the field of solar cells[18]. As we all know, no studies on synthesize Cu_2CdSnS_4-CdS nanocomposites and further test photocatalytic activity have been published till now.

Here, a novel two-step solvothermal method is adopted to prepare Cu_2CdSnS_4-CdS nanocomposites. Then the photocatalytic performance of the obtained Cu_2CdSnS_4-CdS nanocomposites is evaluated via the photocatalytic degradation of RhB under visible light illumination.

2. Experimental details

All chemical reagents, including Cupric nitrate ($Cu(NO_3)_2 \cdot 3H_2O$), Cadmium dichloride ($CdCl_2 \cdot 2.5H_2O$), Tin dichloride ($SnCl_2 \cdot 2H_2O$) and Thiocarbamide (H_2NCSNH_2), are received from Nanshi-Reagent Corp., and all materials do not need to be further purified. In the present experiment, Cupric nitrate (2mMol), Cadmium dichloride (1mMol), Tin dichloride (1mMol) and Thiocarbamide (6mMol) are dissolved in 80ml ethylene glycol(EG) as precursor. A clear solution is obtained after stirring for 2h, then the solution is transferred into autoclaves of 100ml capacity and heated at 200℃ for 12h. The black precipitation are washed and centrifuged several times with deionized water after cooling down to room temperature, and followed drying in vacuum at 80℃ for 3h for further use. Moreover, Cadmium dichloride(1mMol) and Thiocarbamide (2mMol) are dissolved in 80ml ethylene glycol(EG) as precursor, and a certain amount of as-obtained Cu_2CdSnS_4 powder above are added. After full stirring, and then the mixture is transferred into autoclaves and heated at 200℃ for 12h, then the products are treated similar with that of pure Cu_2CdSnS_4 nanoparticles to finally obtain the Cu_2CdSnS_4-CdS nanocomposites.

The structural characteristics of all the prepared samples are recorded using powder X-ray diffractometer (XRD, PaNalytical X'Pert Pro). The surface morphologies are analyzed using scanning electron microscopy (SEM, LEO-1530VP). The photoluminescence spectra are performed with a photoluminescence detector (PL, PerkinElmer LS-55). The room temperature optical and photocatalytic activities are calculated corresponding UV-visible spectra by using Shimadzu UV2450 spectrophotometer.

3. Results and discussion

Fig.1 exhibits the XRD patterns for as-prepared Cu_2CdSnS_4, CdS and Cu_2CdSnS_4-CdS nanoparticles. We can not observe other characteristic peaks belonging to other impurity phases except for those of Cu_2CdSnS_4 and CdS structure. For Cu_2CdSnS_4, the strong diffraction peaks observed at values 2θ = 27.8°, 46.7° and 56.1° consistent with (112), (220) and (312) plans being assigned to its cernyite structure (JCPDS No. 29-0537). The crystallite size is calculated as about 45nm from the (112) peak using the Debye-Scherer's formula. For CdS, the main diffraction peaks at 2θ =25.4°, 26.5°, 28.2°, 43.8° and 52.1° correspond to (100), (111), (101), (220) and (311) plans being assigned to its zinc blende structure (JCPDS No. 10-0454) and wutzite structure (JCPDS No. 41-1049), respectively. It is concluded that CdS mixed crystal is obtained, indicating the high separation ability of photon-generated carriers. For pure CdS, the average grain size is obtained as ~80nm. In the case of all samples, the peaks of pure CdS are noticeably strong as compared to those of Cu_2CdSnS_4-CdS for CdS phase due to CdS being partly shielded by Cu_2CdSnS_4 during the synthesis process. It is also seen that the peaks of Cu_2CdSnS_4 phase are strong as compared to that of CdS phase in the composite materials. Meanwhile, Cu_2CdSnS_4 nanocrystals with (220) preferred orientation growth because of the addition of CdS are investigated during the synthesis process.

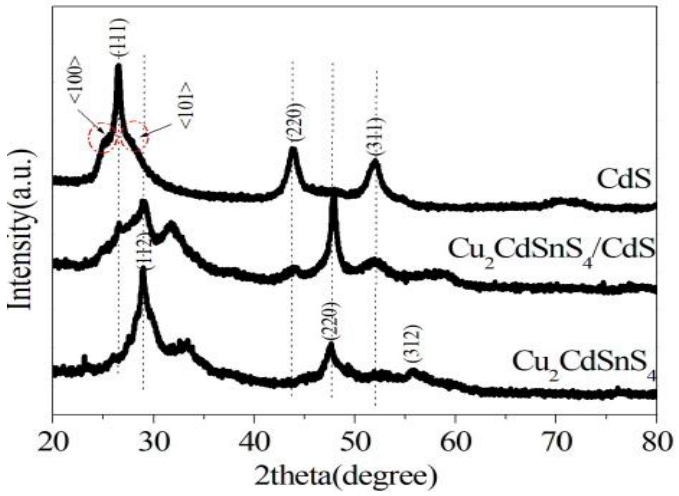

Fig. 1. XRD patterns of Cu_2CdSnS_4, CdS and Cu_2CdSnS_4-CdS samples.

The micro-morphologies of all as-prepared Cu_2CdSnS_4, CdS and Cu_2CdSnS_4-CdS materials are investigated. As observed in Fig.2, pristine CdS are constituted of spheroid nanoparticles with an average diameter of 100nm, while for pristine Cu_2CdSnS_4, nanoflower structure self-assembling by nanosheets with a thickness of ~50nm are observed, in agreement with the literature report[19].

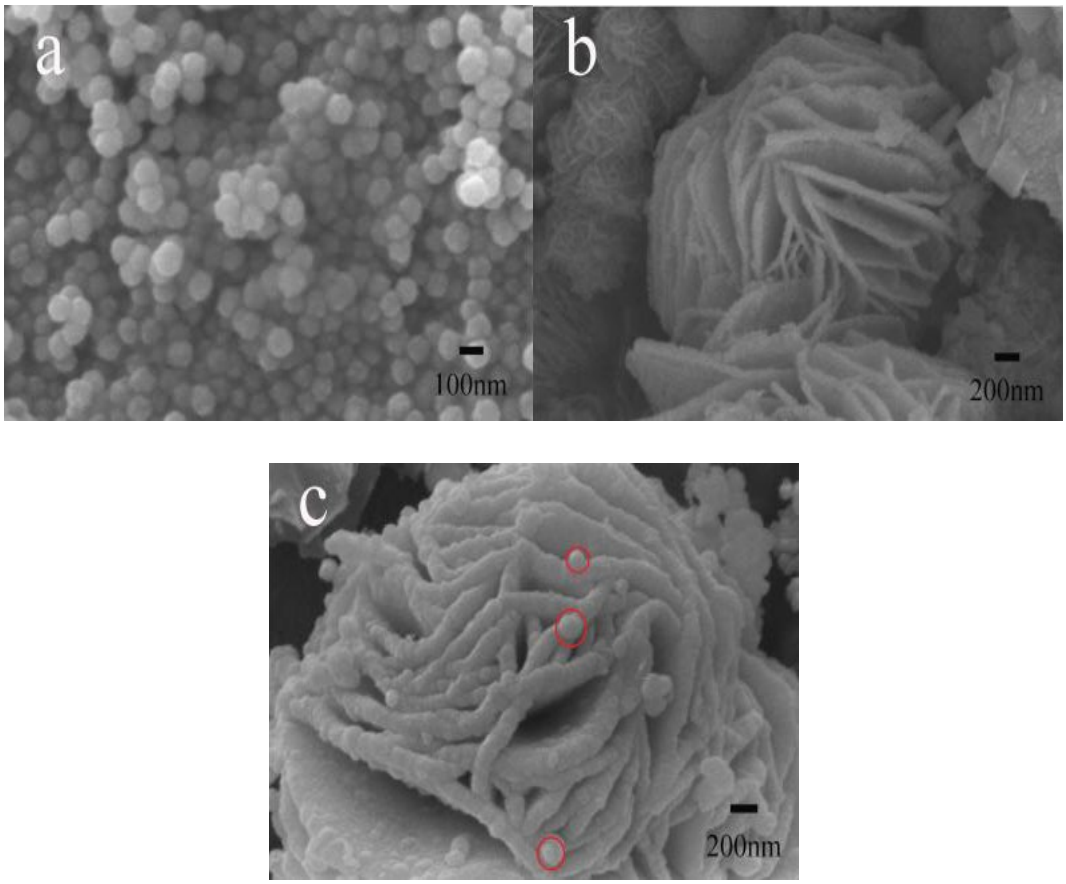

Fig. 2. SEM images of (a)CdS, (b)Cu_2CdSnS_4 and (c)Cu_2CdSnS_4-CdS samples.

For Cu_2CdSnS_4-CdS composites, the thickness of the petal is about 150nm, while CdS crystals grow on the surface of the Cu_2CdSnS_4 petal during their chemical synthesis process.

Fig.3 display the optical band gap energies calculation of as-prepared Cu_2CdSnS_4, CdS and Cu_2CdSnS_4-CdS materials. It is worth noting that the determined band gap value of Cu_2CdSnS_4 is 1.43eV while that of the CdS band gap is found to be 2.33eV, which is in consistent with those reported values in literature[20-21]. For Cu_2CdSnS_4-CdS composites, the band gap is around 1.5eV, which is conducive for the application of excellent photocatalyst.

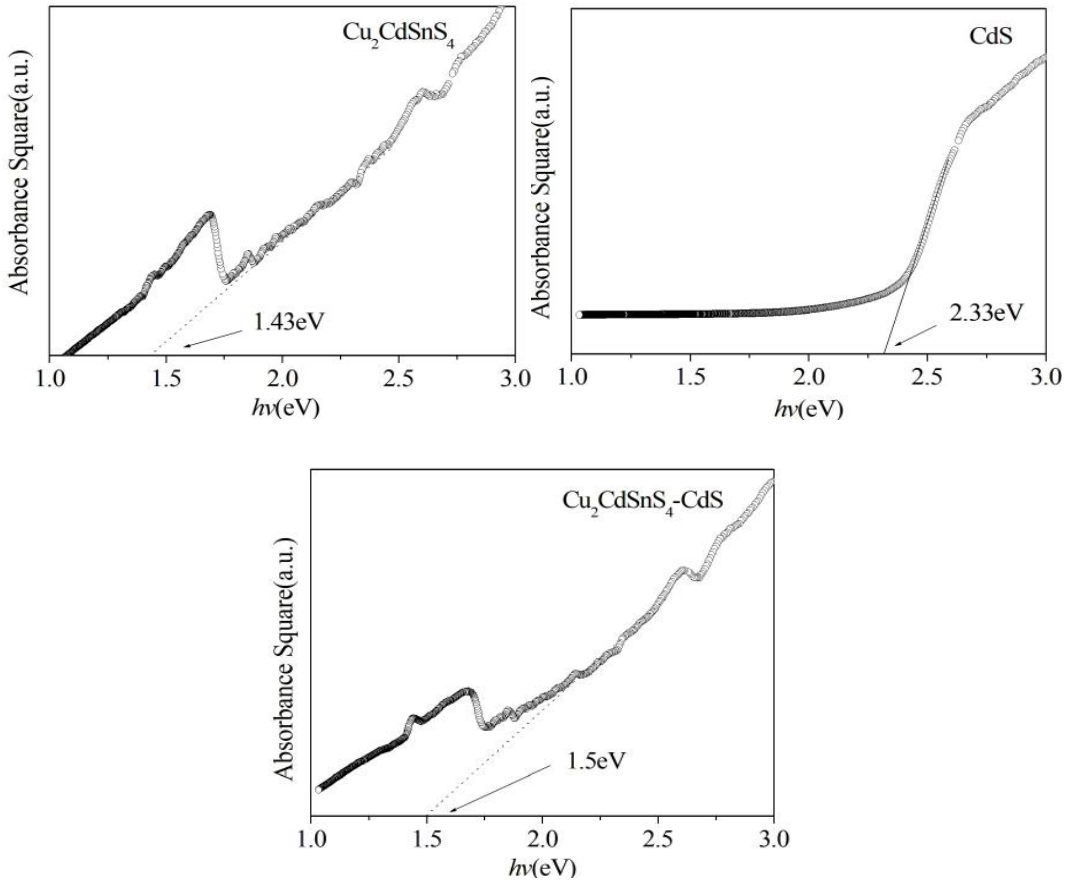

Fig. 3. Optical bandgap estimation of Cu_2CdSnS_4, CdS and Cu_2CdSnS_4-CdS samples.

For photocatalyst, the PL technique may be used to evaluate the recombination rate of the products. The PL spectra of Cu_2CdSnS_4, CdS and Cu_2CdSnS_4-CdS can be displayed in Fig.4. Cu_2CdSnS_4-CdS composites exhibit the lower emission intensity compared with pure Cu_2CdSnS_4 and CdS. It is evidence that the recombination rate of photoexcited electrons and holes is effectively inhibited by Cu_2CdSnS_4-CdS composites. Therefore, the close contact of Cu_2CdSnS_4 and CdS contribute to significantly improvement of the separation efficiency of photoproduced electrons and holes. It demonstrates that Cu_2CdSnS_4-CdS composites have high photocatalytic performance.

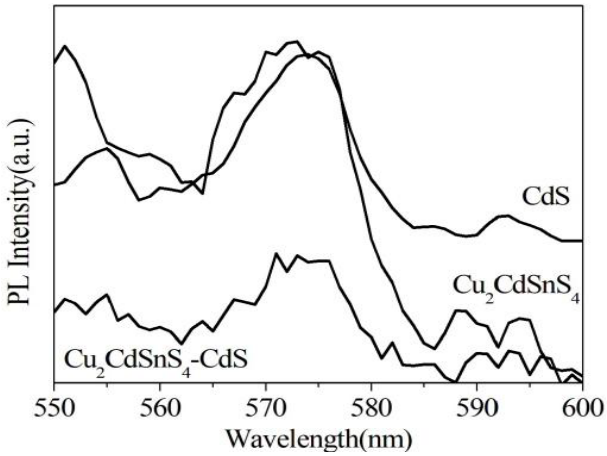

Fig. 4. Photoluminescence spectra of Cu_2CdSnS_4, CdS and Cu_2CdSnS_4-CdS samples.

As the target pollutant, RhB is degraded for different time under visible-light irradiation to explore the photocatalytic performance of all synthesized samples, As we all know, RhB can not be degraded under condition of absence of photocatalysts. As exhibited in Fig.5(a). It can be seen that Cu_2CdSnS_4-CdS nanocomposites exhibit high photodegradation efficiency compared to pristine Cu_2CdSnS_4 and CdS. After irradiation of 100 min, the photodegradation efficiency of Cu_2CdSnS_4-CdS nanocomposites is reached to 94%. Besides, the reationship between photocatalytic reaction kinetic curves and catalytic reaction time over the obtained photocatalysts are shown in Fig.5(b). The reaction data are fitted by the pseudo-first-order reaction kinetics model[22]: $\ln(C_0/C) = kt+b$, where k, C_0 and C are the apparent first-order rate constant and RhB dye concentrations at times 0 min and t min, respectively. The corresponding photodegradation of RhB constants k are estimated to be $0.0204min^{-1}$, $0.0113min^{-1}$and $0.0255min^{-1}$ for Cu_2CdSnS_4, CdS and Cu_2CdSnS_4-CdS, respectively. It is clear that Cu_2CdSnS_4-CdS nanocomposites exhibit the highest reaction rate, inducing the best photocatalytic performance. Based on the results of discussions and analysis above, the photocatalytic mechanism of Cu_2CdSnS_4-CdS nanocomposites are elucidated in Fig.6. Cu_2CdSnS_4 and CdS are stimulated to generate electron-hole pairs under the visible light conditions. When Cu_2CdSnS_4 and CdS are in contact, the photo-generated electrons would transfer from Cu_2CdSnS_4 to CdS, while the photo-generated holes of CdS would spontaneously flow towards Cu_2CdSnS_4, resulting in an efficient separation of the photoproduced electrons and holes. The photo-generated holes in the VB of Cu_2CdSnS_4 section react with OH^- or H_2O to produce •OH [23]. Similarly, the photo-generated electrons in the CB of CdS section react with O_2 and H_2O to produce •OH. The RhB dye can be degraded directly because of reaction between •OH and RhB dye.

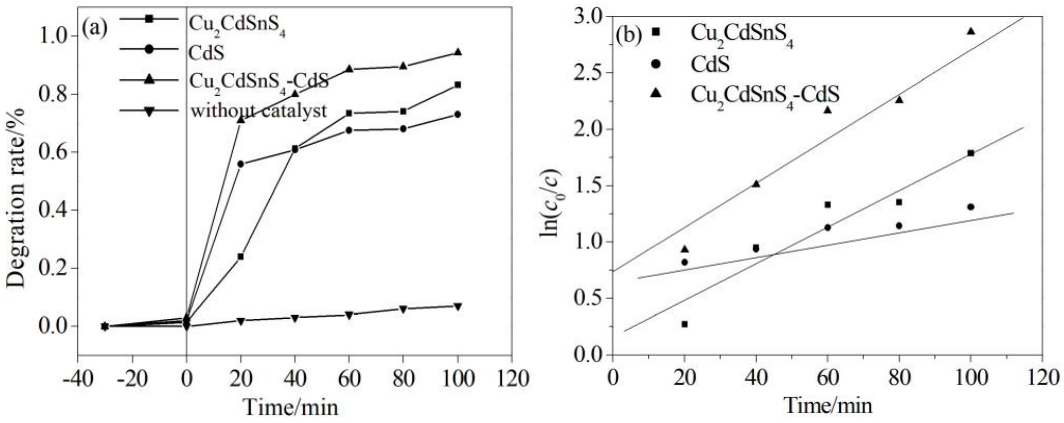

Fig. 5. (a) The degradation rate (b) $ln(c_0/c)$ as a function of different time of Cu_2CdSnS_4, CdS and Cu_2CdSnS_4-CdS samples.

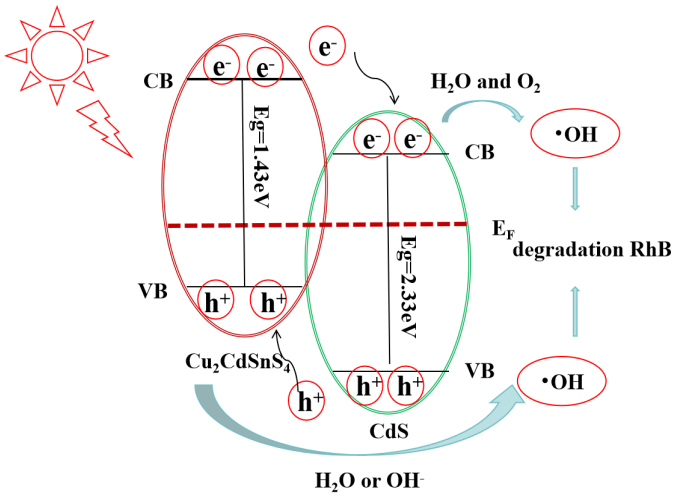

Fig. 6. Basic mechanism of photocatalytic reactions of Cu_2CdSnS_4-CdS nanocomposites.

4. Conclusion

In this work, a novel Cu_2CdSnS_4-CdS nanocomposites is successfully prepared by a two-step solvothermal method. It is shown to be composed of flower-like nanoparticles with the petal thickness of ~50nm and spheroid structure with the average size of 100nm. The optical bandgap of the Cu_2CdSnS_4-CdS composites nanoparticles is around 1.5eV. Comparing to pure Cu_2CdSnS_4 and CdS under light conditions, Cu_2CdSnS_4-CdS composites exhibit enhanced photocatalytic activities for degradation of RhB. The study provides a simple way to synthesis Cu_2CdSnS_4-CdS composites for optimum visible-light photocatalyst.

References

[1] H. Katagiri, K. Saitoh, T. Washio, H. Shinohara, T. Kurumadani, S. Miyajima, Sol. Energy Mater. Sol. Cells **65**,141 (2001); https://doi:10.1016/S0927-0248(00)00088-X
[2] W. G. Zhao, G. Wang, Q. G. Tian, L.J. Huang, S. Gao, D. C. Pan, Sol. Energy Mater. Sol. Cells, 133,**15** (2015); https://doi.org/10.1016/j.solmat.2014.10.040
[3] Y. Cui, G. Wang, D. C. Pan, J. Mater. Chem. **22**, 12471 (2012); https://doi.org/10.1039/C2JM32034G
[4] H. Guan, Y. F. Shi, H. J. Hou, Xu Wang, F. L. Yu, Micro Nano Lett. **9**, 251 (2014); https: // doi. org/10.1049/mnl.2013.0686
[5] M. Rouchdi, E. Salmani, N. Hassanain, A. Mzerd, Opt. Quant. Electron. **49**, 165 (2017); http://doi:10.1007/s11082-017-1005-8
[6] Q. Zhang, H. M. Deng, L. L. Chen, J. H. Tao, J. J. Yu, P. X. Yang, J. H. Chu, Mater. Lett. **193**, 206 (2017); https://doi.org/10.1016/j.matlet.2017.02.002
[7] M. Cao, L. Li, W. Z. Fan, X. Y. Liu, Y. Sun, Y. Shen, Chem. Phys. Lett. **534**, 34 (2012); https://doi.org/10.1016/j.cplett.2012.03.016
[8] K. Mokurala, S. Mallick, RSC Adv. **7**, 15139 (2017); https://doi.org /10.1039 /C7RA90044A
[9] L. Y. Nie, S. Liu, Y. Q. Chai, R. Yuan, J. Anal. Appl. Pyrol. **112**, 363 (2015); https://doi.org/10.1016/j.jaap.2014.12.020
[10] J. Henry, P. Prema, D. P. Padiyan, K. Mohanraj, G. Sivakumar, New J Chem. **40**, 2609 (2016); https://doi.org/10.1039/C5NJ03154K
[11] L. W. Wang, Z. Liu, J. H. Han, R. P. Li, M. J. Huang, Nanoscale Res. Lett. **14**, 148 (2019); https://doi.org/10.1186/s11671-019-2977-z
[12] S. Sweety, M. B. Moses, D. M. Mison, R. S. Chandra, J. Nanosci. Nanotechno. **18**, 1369 (2018); https://doi.org/10.1166/jnn.2018.15208
[13] E. Esakkiraj, S. P. Sheik Abdul Kadhar, J. Henry, K. Mohanraj, S. Kannan, S. Barathan, G. Sivakumar, Optik **124**, 5229 (2013); https://doi.org/10.1016/j.ijleo.2013.04.003
[14] S. Mageswari, L. Dhivya, B. Palanivel, R. Murugan, J. Alloy. Compd. **545**, 41 (2012); https:// doi. org/10.1016/j.jallcom.2012.08.010
[15] Q. Zhao, R. F. Liu, Y. L. Shen, M. L. Fang, M. F. Dong, J. Nanosci. Nanotechno. **18**, 4755 (2018); https://doi.org/10.1166/jnn.2018.15344
[16] E. Hernández-Rodríguez, M. Loeza-Poot, I. Riech, V. Rejón, J. L. Peña, J. Phys. D: Appl. Phys. **48**, 255102 (2015); https://doi:10.1088/0022-3727/48/25/255102
[17] N. Ghows, M. H. Entezari, Ultrason. Sonochem. 18, **269** (2011); https://doi.org/10.1016/j.ultsonch.2010.06.008
[18] H. F. Guo, Y. Li, X. Fang, K. Z. Zhang, J. N. Ding, N. Y. Yuan, Mater. Lett. **162**, 97 (2016); https://doi.org/10.1016/j.matlet.2015.09.112
[19] Q. F. Xu, Z. Y. Wang, H. Yang, Y. J. Xiang, G. J. Nie, W. J. Yue, J. Alloy. Compd. **904**, 163966 (2022); https://doi.org/10.1016/j.jallcom.2022.163966
[20] C. Li, M. Cao, J. Huang, L. J. Wang, Y. Shen, Mater. Lett. **140**, 170 (2015); https:// doi. org/ 10.1016/j.matlet.2014.10.165
[21] W. J. Zhu, L. K. Yang, F. Liu, Z. J. Si, M. J. Hou, Z. J. Li, Z. Chen, J. Alloy. Compd. **973**, 172747 (2022); https://doi.org/10.1016/j.jallcom.2023.172747

[22] X. W. Lu, X. Z. Li, F. Chen, Z. G. Chen, J. Qian, Q. F. Zhang, J. Alloys Compd. **815**, 152326 (2020); https://doi.org/10.1016/j.jallcom.2019.152326
[23] I. Zgura, N. Preda, G. Socol, C. Ghica, D. Ghica, M. Enculescu, I. Negut, L. Nedelcu, L. Frunza, C.P. Ganea, S. Frunza, Mater. Res. Bull. **99**, 174 (2018); https://doi.org/10.1016/j.materresbull.2017.11.013